Volume 12
Number 9
7 March 2024
Pages 3017–3380

Journal of Materials Chemistry C

Materials for optical, magnetic and electronic devices

rsc.li/materials-c

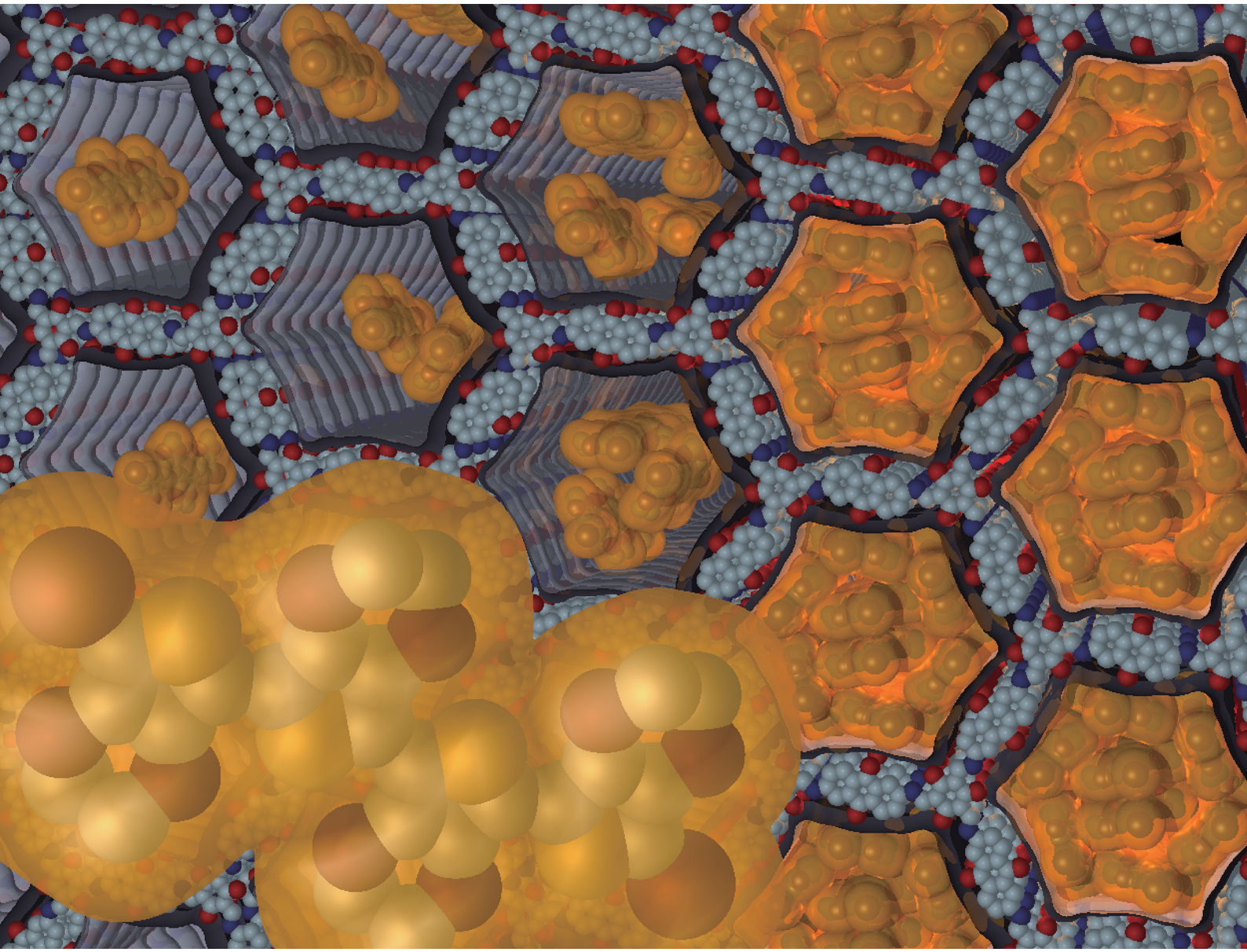

ISSN 2050-7526

ROYAL SOCIETY OF CHEMISTRY

PAPER

Kunio Awaga *et al.*

Critical transition to a highly conductive state through PEDOT oligomer percolation in redox-active COFs

Journal of Materials Chemistry C

ROYAL SOCIETY OF CHEMISTRY

PAPER

View Article Online
View Journal | View Issue

Cite this: J. Mater. Chem. C, 2024, 12, 3072

Critical transition to a highly conductive state through PEDOT oligomer percolation in redox-active COFs†

Chaoqun Cao,[a] Qi Chen,[a] Rie Suizu [ab] and Kunio Awaga *[a]

Received 28th December 2023,
Accepted 5th February 2024

DOI: 10.1039/d3tc04794f

rsc.li/materials-c

Covalent organic frameworks (COFs) have garnered significant attention in recent years, but they generally suffer from low electrical conductivity. In our previous studies, we observed that the nano-hybrid material PEDOT@AQ-COF (PEDOT = poly(3,4-ethylenedioxythiophene) and AQ-COF = ketoenamine-linked COF with anthraquinone (AQ) moieties), formed by polymerizing the organic conductive polymer PEDOT within the hollow pores of a COF, demonstrates outstanding electrical conductivity and energy storage properties. In this study, we systematically synthesized samples with various ratios of PEDOT to AQ-COF by adjusting the concentration of the precursor molecule in AQ-COF. Elemental analysis results indicated that PEDOT exists as oligomers with a degree of polymerization between 3.4 and 5.6, and there is a saturation point for the amount of PEDOT. This saturation state suggests that the PEDOT chains are densely packed within the cavity of AQ-COF, forming molecular contacts between PEDOT and AQ-COF. We assessed the electrical conductivity, electrochemical properties, and electron paramagnetic resonance (EPR) of the PEDOT@AQ-COF series. We observed that, upon reaching the saturation point of PEDOT, a critical transition occurs to a highly conductive state. In this state, the cyclic voltammetry curves exhibit redox reactions of AQ-COF, assisted by the PEDOT guest molecules. Compared to the low-conductivity sample, the high-conductivity samples in EPR displayed a broader linewidth component with nearly temperature-independent spin susceptibility.

Introduction

Covalent organic frameworks (COFs) are a fascinating class of materials that have garnered significant attention in recent years. These intricate structures, composed of organic building blocks, are expected to exhibit remarkable properties and offer immense potential for diverse applications. Benefitting from their tunable porosity, high surface area, and structural topology, COFs have emerged as promising candidates for catalysis,[1–4] gas storage,[5,6] and sensing.[7,8] They are also attracting much attention as energy storage materials, particularly for application in rechargeable batteries and capacitors,[7–12] due to their porosity, which allows for ion penetration, as well as their potential for chemical modifications to enhance redox activity.

However, the early COFs, especially linked with boronate esters, suffered from poor hydrolytic and oxidative stability, limiting applications in energy storage.[13] To improve their chemical stability, Banerjee *et al.* developed β-ketoenamine-linked COFs *via* a Schiff base reaction,[14,15] which showed strong resistance toward acids, bases, and boiling water. At the same time, the Dichtel group incorporated redox-active anthraquinone (AQ) moieties into a ketoenamine-linked COF (AQ-COF), which exhibited a reversible faradaic process in a H_2SO_4 electrolyte. It is worth noting that the AQ-COF yielded a limited capacitance of 48 F g^{-1} even at a low current density of 0.1 A g^{-1}. This capacitance was significantly enhanced to 197 F g^{-1} by electropolymerizing EDOT (3,4-ethylenedioxythiophene) within AQ-COF.[9] Although this strategy improves the conductivity of AQ-COF thin films, the surface polymerization of EDOT may hinder further penetration of EDOT when applied to bulk COFs. To address these challenges, our group has proposed an alternative approach to polymerize DBrEDOT (see Scheme 1a) in the AQ-COF pore. Specifically, we utilized AQ-COF as the matrix framework and successfully impregnated the PEDOT precursor, DBrEDOT (2,5-dibromo-3,4-ethylenedioxythiophene).[16] Then, solid-state polymerization of PEDOT at high temperature (60–85 °C), while preserving the integrity of the underlying framework. The obtained PEDOT@AQ-COF composite exhibited an electrical conductivity of as high as 1 S cm^{-1},

[a] Department of Chemistry & Integrated Research Consortium on Chemical Sciences (IRCCS), Nagoya University, Furo-cho, Chikusa-ku, Nagoya, 464-8601, Japan. E-mail: awaga.kunio.h8@f.mail.nagoya-u.ac.jp
[b] Japan Science and Technology Agency (JST), PRESTO, 4-1-8 Honcho, Kawaguchi, Saitama 332-0012, Japan

† Electronic supplementary information (ESI) available: Details of material preparations and characterizations. See DOI: https://doi.org/10.1039/d3tc04794f

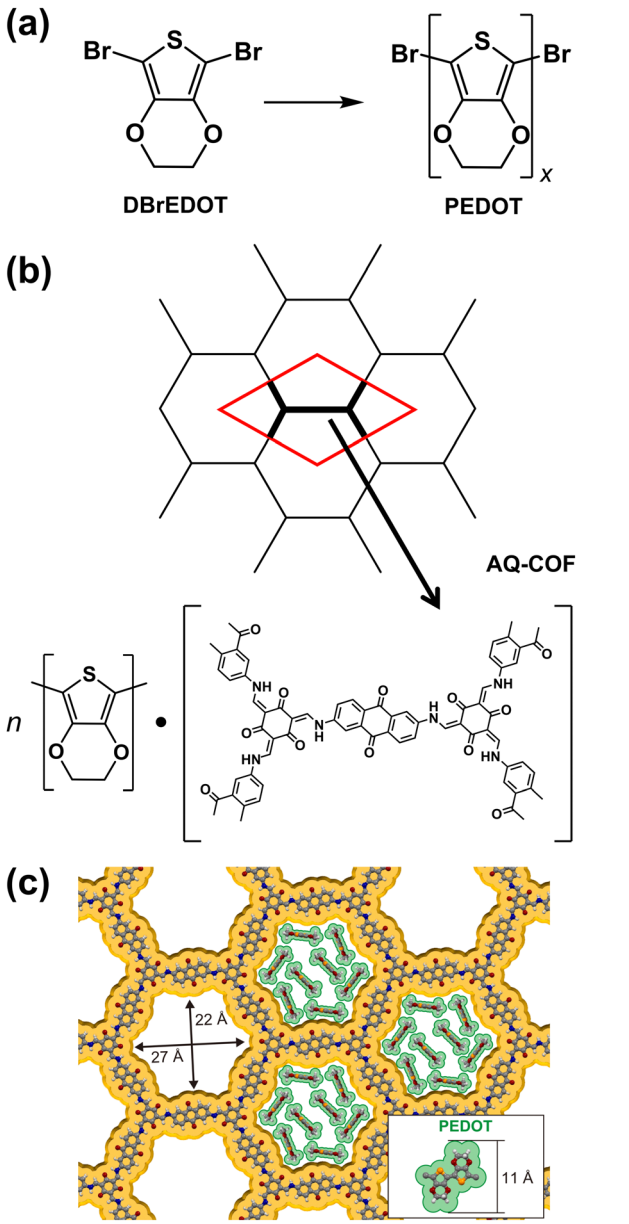

Scheme 1 (a) Molecular structures of DBrEDOT and PEDOT. (b) Honeycomb framework of AQ-COF and chemical formula of the repeating unit shown as the red rhombus. (c) Top view of AQ-COF and the expected close packing of PEDOT in it.

leading to a high capacitance of 1663 F g^{-1} at a current density of 1 A g^{-1}.[16]

In this study, we prepared seven PEDOT@AQ-COF samples by varying the ratio of guest and host components, to elucidate the conducting mechanism and the host–guest interaction in PEDOT@AQ-COF. We found that the number of PEDOT chains in a 1D channel of AQ-COF increases from 4 to 8, in which there was a critical threshold number to switch the conductivity from low to high. The CV curves, the *I*–*V* curves and the EPR spectra of PEDOT@AQ-COF also exhibited significant changes at this critical point.

Results and discussion

Samples

AQ-COF was synthesized following the reported method.[10] The host–guest hybrid material PEDOT@AQ-COF was prepared using a method previously described by our group. Specifically, we dissolved the precursor compound DBrEDOT in acetone containing AQ-COF and allowed for intercalation by stirring the suspension. Subsequently, we obtained DBrEDOT@AQ-COF by evaporating the acetone and washed the sample with hexane to remove excess DBrEDOT from the surface. Through thermal treatment for polymerization in DBrEDOT@AQ-COF, we obtained black-colored PEDOT@AQ-COF. The details of the sample preparations and characterizations are described in the ESI† (Fig. S1–S5). It is noteworthy that the BET surface area of the AQ-COF prepared in this study was 851 m^2 g^{-1} (refer to Fig. S4, ESI†). Although this value was two-thirds of that reported in our previous study (ref. 16), we consistently employed this AQ-COF sample as the host for PEDOT in the current investigation.

We prepared seven PEDOT@AQ-COF samples by varying the initial weight of DBrEDOT relative to 200 mg of AQ-COF, as listed in Table 1. This table presents the results of elemental analysis for them. Because of an error bar of ±0.3% in the elemental analysis, the results exhibit some scattering. Nonetheless, we recognized that the bromine percentages in the seven samples were rather high, ranging from 8 to 13%, without systematic dependence on the sample numbers. Note that the bromine concentration in DBrEDOT is 53%, and it should decrease with the PEDOT polymerization. Assuming a chemical formula of Br(-EDOT-)$_x$Br for PEDOT, we estimated the *x* values, namely the lengths of the PEDOT chains, from the S/Br ratios, and listed the results in Table 1. It was found that there was no systematic dependence of *x* on the initial concentration of DBrEDOT; the *x* values stayed between 3.4 and 5.6. This means that the PEDOT species should be regarded as oligomers[17] rather than infinite polymers in the present PEDOT@AQ-COFs, and furthermore that the length of the oligomers, namely *x*, depends little on the initial amount of the precursor compound DBrEDOT.

Furthermore, the concentration of sulphur, derived exclusively from PEDOT, implies a rise in PEDOT content with greater initial weights of DBrDOT. Since the nitrogen component is derived solely from AQ-COF, we calculated the molar

Table 1 The results of the elemental analysis and estimated values of *x* and *n* for samples 1–7. The definitions of *x* and *n* are shown in Scheme 1a and b, respectively

Sample	Weight of DBrDOT/mg	Elemental analysis/%					*x*	*n*
		C	H	N	S	Br		
1	270	50.65	3.12	4.04	6.90	7.65	4.5	4.5
2	300	49.30	3.34	3.42	8.06	8.95	4.5	6.2
3	330	48.94	3.40	3.53	8.99	8.05	5.6	6.7
4	360	44.86	3.26	2.85	8.44	12.28	3.4	7.8
5	390	44.32	3.36	2.97	9.02	13.23	3.4	8.0
6	420	48.08	3.25	3.11	9.05	8.30	5.4	7.6
7	450	46.47	3.35	2.98	9.54	10.01	4.8	8.3

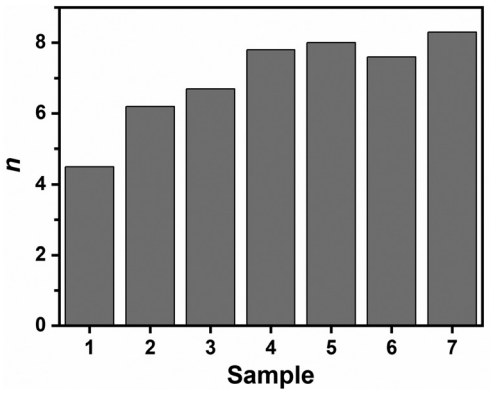

Fig. 1 Sample dependence of the molar ratio n between EDOT and the unit cell of AQ-COF, calculated from the results of the elemental analysis.

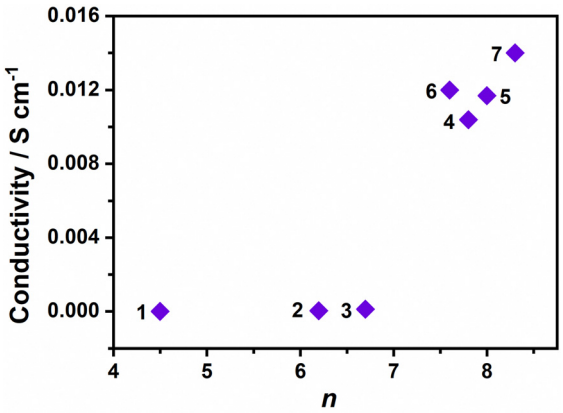

Fig. 2 Room-temperature conductivity for samples 1–7.

ratio between the repeating units of PEDOT and AQ-COF, namely between EDOT and a part of the AQ-COF framework (see Scheme 1b). Through the S/N ratio, we calculated the n values in n[EDOT]·[AQ-COF], where [EDOT] is based on the chemical formula of $C_6H_4O_2S$ and [AQ-COF] is based on the chemical formula of $C_{60}H_{30}N_6O_{12}$. Fig. 1 shows the n values for the seven samples; in the order of the sample number, the n values increase from 4.5 to 8, and demonstrate saturation after sample 4. It is worth noting that the volume of the unit cell in the honeycomb lattice is identical to that of its hexagonal pore. Given that the thickness of the AQ-COF honeycomb layer is almost the same as the length of the repeating unit EDOT, the n value roughly corresponds to the number of PEDOT chains within a single channel of the honeycomb AQ-COF. We also estimated the maximum number of PEDOT chains in a hexagonal channel of AQ-COF to be eight (see Scheme 1c). This estimation was based on the calculation of the cross-sectional areas for the hexagonal pore (445.5 nm^2) and the EDOT molecule (50 nm^2). Interestingly, this value closely aligns with the saturation value obtained from the elemental analysis. Scheme 1c illustrates the anticipated close packing of the PEDOT chains with the hexagonal channel in AQ-COF, which suggests intermolecular contacts between the PEDOT chains and the AQ-COF framework in samples 4–7.

Electrical conductivity

The room-temperature conductivity of the seven samples 1 –7 were measured using a homemade instrument employing a two-probe method. The results are illustrated in Fig. 2, with the horizontal axis representing the n values (see Fig. S6 and S7, ESI†). When $n \leq 6.7$, the samples exhibit low conductivities on the order of 10^{-4} S cm^{-1} or lower, while, when $n \geq 7.7$, they demonstrate high conductivities of 10^{-2} S cm^{-1} or higher. A significant increase in conductivity is observed in a narrow region of $6.7 \leq n \leq 7.7$. It is important to note that this transition occurs in these samples, even though there is no significant change in the PEDOT length.

The temperature dependence of the conductivity σ was measured for samples 3 and 4. The results are shown in Fig. S8 (ESI†), indicating linear relations between ln σ and $1/T$ for them. These dependences were interpreted by the Arrhenius equation, $\sigma = \sigma_0 \exp(-\Delta/k_BT)$, where σ_0 is the pre-exponential factor, Δ is the activation energy and k_B is the Boltzmann constant. The parameters were calculated to be $\sigma_0 = 2.6 \times 10^{-2}$ S cm^{-1} and $\Delta = 0.16$ eV for sample 3, and $\sigma_0 = 6.4 \times 10^{-1}$ S cm^{-1} and $\Delta = 0.08$ eV for sample 4, respectively. It is notable that the value of Δ for sample 4 is nearly half of that for sample 3, and σ_0 for sample 4 is larger than that for sample 3 by one order of magnitude.

Fig. S14 (ESI†) shows the Kubelka–Munk functions of samples 3 and 4, and AQ-COF, obtained by the reflection measurements. They correspond to absorption spectra, showing that AQ-COF has no absorption at all in the NIR region, while samples 3 and 4 have broad absorption in this region. Also, although the electrical conductivities of samples 3 and 4 are very different, there is no noticeable difference in these spectra.

Cyclic voltammetry

Cyclic voltammetry (CV) was examined for samples 1–7 using three-electrode cells that contained a 1 M H_2SO_4 supporting electrolyte. The potential was swept in the range from −0.2 to 0.6 V relative to the Ag/AgCl reference electrode. The results are shown in Fig. 3a, where samples 1–3 simply exhibit capacitive behaviour with quasi-rectangular-shaped curves. In contrast, the CV curves of samples 4–7 exhibit large oxidative and reductive peaks due to a reversible faradaic reaction, in addition to capacitive behaviour. The present redox potential of −0.03 V *vs.* Ag/AgCl indicates that this reaction occurs on the anthraquinone moiety in AQ-COF. Electrochemical impedance spectroscopy (EIS) measurements were conducted for selected samples (see Fig. S15, ESI†).

By integrating the CV curves, we calculated the capacitance involved in the capacitive/redox behaviour for samples 1–7. The results are shown in Fig. 3b. There is a significant change in the capacitance between samples 3 and 4, which corresponds to a change in conductivity (see Fig. 2). It is concluded that, while the low conductive PEDOT@AQ-COFs (samples 1–3) exhibit only capacitive behaviour, AQ-COF exhibits the redox reaction in the high conductive ones (samples 4–7). It is thought that the PEDOT involved in the COF would play the role of a conductive pathway between the electrodes and AQ-COF. It is noteworthy

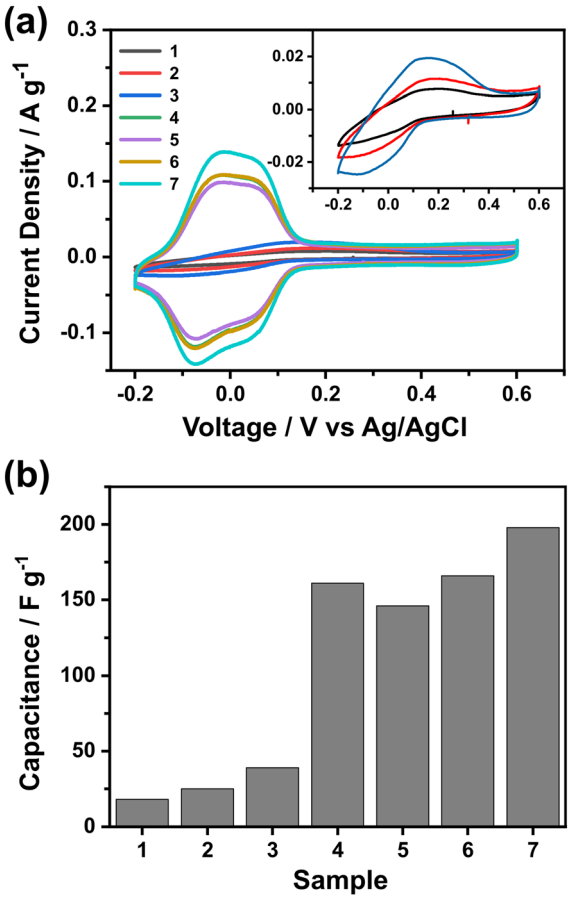

Fig. 3 (a) CV curves of samples 1–7 at a scan rate of 5 mV s^{-1}. The inset shows the results for samples 1–3 in an enlarged scale. (b) Sample dependence of the capacitance, obtained by integrating the CV curves.

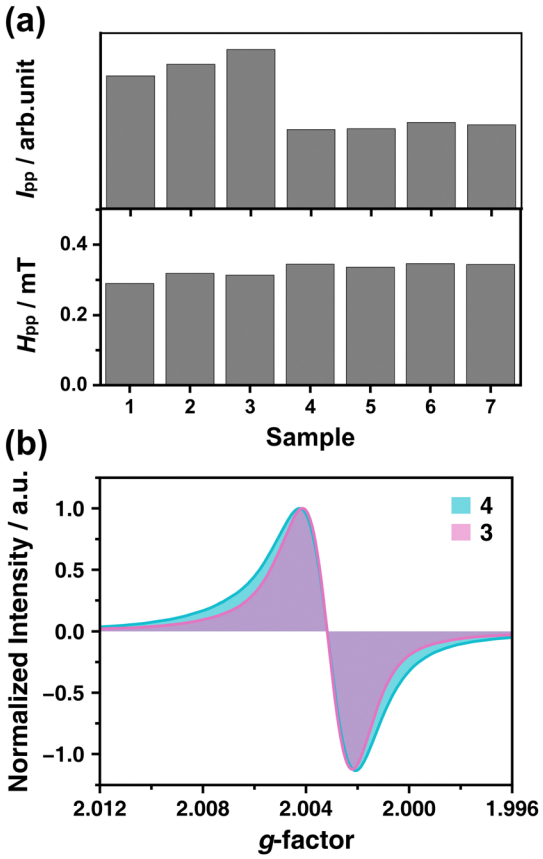

Fig. 4 (a) The line height and line width of the EPR spectra for samples 1–7. (b) EPR spectra of samples 3 and 4.

that the conductivities and capacitances of samples 4–7 are significantly lower than those reported in our previous data (ref. 16). This is likely attributed to the considerably smaller surface area of the AQ-COF used in this study compared to the previous one.

EPR spectroscopy

Room temperature EPR was measured for the seven samples, each with a quantity of 2 mg; their spectra are shown in Fig. S9 (ESI†). Samples 1–7 exhibited strong EPR signals at $g \approx 2.003$ at room temperature. Note that the host compound, AQ-COF, exhibits a very weak EPR signal, likely attributable to paramagnetic lattice defects (Fig. S10, ESI†), while PEDOT displays an EPR signal at $g = 2.006$ at room temperature.[18] It is also noteworthy that conductive polymers, such as PEDOT, typically contain both dication and radical cation charge carriers, with the latter displaying strong EPR signals. The line-shape of these signals depends on the doping level. Fig. 4 shows a comparison of the room-temperature EPR signals among the seven samples based on the peak-to-peak line height I_{pp}, and the peak-to-peak line width H_{pp}. Although a significant difference cannot be seen in H_{pp} between the low conductive samples 1–3 and the high conductive samples 4–7, I_{pp} of the latter is nearly half of those of the former. Fig. 4b shows a comparison between the EPR line shapes of samples 3 and 4; it is clear that the EPR signal of the high-conductive sample 4 contains a broad-line component that is assignable to conductive electrons.

The temperature dependence of EPR was measured in the temperature range between 10 and 300 K for the low conductive sample 1 and the high conductive sample 4. The EPR spectra for them are shown in Fig. S11 and S13 (ESI†). There was no significant difference in the g factor between the two samples in the whole temperature range; their signals exhibited g factors of *ca.* 2.004. Fig. 5 shows the relationship between spin susceptibility (intensity) χ_{EPR} both temperature and its inverse for the two samples. It is found that χ_{EPR} of the low conductive sample 1 nearly follows the Curie law $\chi_{EPR} = C/T$, where C is the Curie constant. The solid line in Fig. 5a is the theoretical one of the Curie law. This behaviour suggests that they are caused by localized paramagnetic lattice defects. In contrast, the temperature dependence of χ_{EPR} of the high-conductive sample 4 cannot be explained by a simple Curie law, but this can be fit to the following equation:

$$\chi_{EPR} = C/T + \chi_0, \quad (1)$$

where the first term expresses the contribution of the paramagnetic lattice defects, and the second term expresses a temperature-independent component for the conductive electrons. The solid line in Fig. 5b is the theoretical one of eqn (1). This analysis clearly

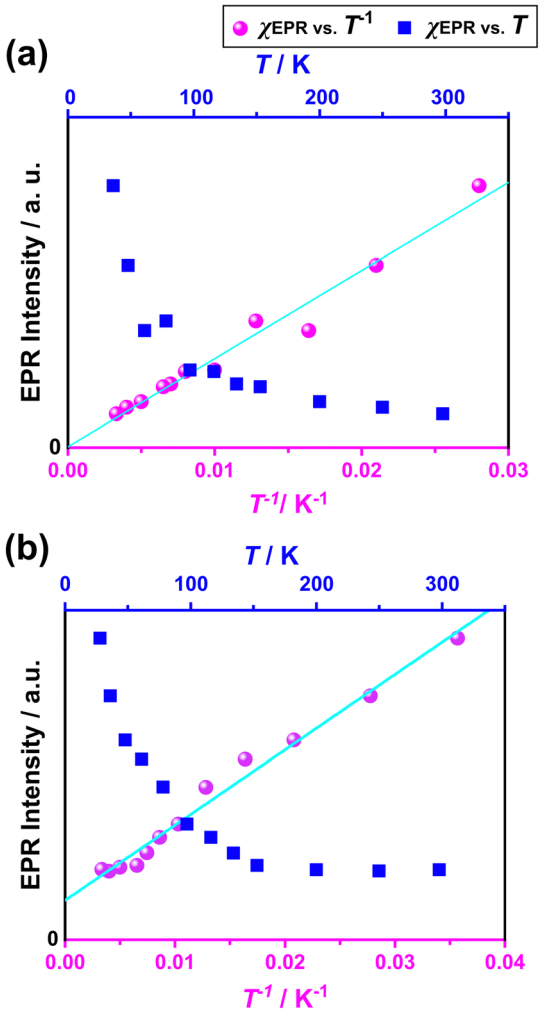

Fig. 5 Temperature dependence of the integrated EPR signal intensity, χ_{EPR} *vs.* T (square) and χ_{EPR} *vs.* T^{-1} (circle), for samples 1 (a) and 4 (b).

suggests the contribution of the highly conductive electrons in 4, which is nearly temperature independent.

Conclusions

In this study, we investigated the physicochemical properties of the PEDOT@AQ-COF system by systematically varying the amount of guest molecule, PEDOT. It was observed that the PEDOT molecules existed as oligomers with approximately $x = 4$ for Br(-EDOT-)$_x$Br in the PEDOT@AQ-COF samples. The amount of PEDOT reached saturation at approximately $n = 8$ for n[EDOT]·[AQ-COF]. This saturation value can be attributed to the close packing structure of the PEDOT guest chains in the hexagonal 1D channel of the AQ-COF host. Upon reaching saturation, there was a rapid increase in electrical conductivity, and the guest PEDOTs were identified to function as nanowires, facilitating the redox process of AQ-COF. The EPRs of the highly conductive samples exhibited a broad-line signal component with an almost temperature-independent χ_{EPR}. These properties are likely a result of the guest–host charge transfer interactions, evident in the PEDOT-saturated samples. We believe that these results will pave the way for achieving high conductivity in porous materials, such as COFs.

Conflicts of interest

There are no conflicts to declare.

Acknowledgements

The authors acknowledge the Japan Society for the Promotion of Science (JSPS) KAKENHI Grants 20H02707 (to R. S.) and 20H05621 (to K. A.), and the Japan Science and Technology Agency (JST) PRESTO Grant JPMJPR21A9 (to R. S.) for funding this work.

Notes and references

1 P. Pachfule, A. Acharjya, J. Roeser, T. Langenhahn, M. Schwarze, R. Schomäcker, A. Thomas and J. Schmidt, *J. Am. Chem. Soc.*, 2018, **140**, 1423–1427.
2 X. Wang, X. Han, J. Zhang, X. Wu, Y. Liu and Y. Cui, *J. Am. Chem. Soc.*, 2016, **138**, 12332–12335.
3 P.-F. Wei, M.-Z. Qi, Z.-P. Wang, S.-Y. Ding, W. Yu, Q. Liu, L.-K. Wang, H.-Z. Wang, W.-K. An and W. Wang, *J. Am. Chem. Soc.*, 2018, **140**, 4623–4631.
4 Y. Wu, H. Xu, X. Chen, J. Gao and D. Jiang, *Chem. Commun.*, 2015, **51**, 10096–10098.
5 X. Guan, Y. Ma, H. Li, Y. Yusran, M. Xue, Q. Fang, Y. Yan, V. Valtchev and S. Qiu, *J. Am. Chem. Soc.*, 2018, **140**, 4494–4498.
6 Y. Zeng, R. Zou and Y. Zhao, *Adv. Mater.*, 2016, **28**, 2855–2873.
7 C. R. DeBlase, K. E. Silberstein, T.-T. Truong, H. D. Abruña and W. R. Dichtel, *J. Am. Chem. Soc.*, 2013, **135**, 16821–16824.
8 A. Halder, M. Ghosh, A. Khayum M, S. Bera, M. Addicoat, H. S. Sasmal, S. Karak, S. Kurungot and R. Banerjee, *J. Am. Chem. Soc.*, 2018, **140**, 10941–10945.
9 C. R. Mulzer, L. Shen, R. P. Bisbey, J. R. McKone, N. Zhang, H. D. Abruña and W. R. Dichtel, *ACS Cent. Sci.*, 2016, **2**, 667–673.
10 S. Wang, Q. Wang, P. Shao, Y. Han, X. Gao, L. Ma, S. Yuan, X. Ma, J. Zhou, X. Feng and B. Wang, *J. Am. Chem. Soc.*, 2017, **139**, 4258–4261.
11 Y. Wu, Z. Zhang, S. Bandow and K. Awaga, *Bull. Chem. Soc. Jpn.*, 2017, **90**, 1382–1387.
12 Q. Xu, S. Dalapati and D. Jiang, *ACS Cent. Sci.*, 2016, **2**, 586–587.
13 J. W. Colson and W. R. Dichtel, *Nat. Chem.*, 2013, **5**, 453–465.
14 B. P. Biswal, S. Chandra, S. Kandambeth, B. Lukose, T. Heine and R. Banerjee, *J. Am. Chem. Soc.*, 2013, **135**, 5328–5331.
15 S. Kandambeth, A. Mallick, B. Lukose, M. V. Mane, T. Heine and R. Banerjee, *J. Am. Chem. Soc.*, 2012, **134**, 19524–19527.
16 Y. Wu, D. Yan, Z. Zhang, M. M. Matsushita and K. Awaga, *ACS Appl. Mater. Interfaces*, 2019, **11**, 7661–7665.
17 K. Onozuka, T. Fujino, R. Kameyama, S. Dekura, K. Yoshimi, T. Nakamura, T. Miyamoto, T. Yamakawa, H. Okamoto, H. Sato, T. Ozaki and H. Mori, *J. Am. Chem. Soc.*, 2023, **145**, 15152–15161.
18 H. Meng, D. F. Perepichka and F. Wudl, *Angew. Chem., Int. Ed.*, 2003, **42**, 658–661.

